

An impedance flow cytometry with integrated dual microneedle for electrical properties characterization of single cell

Muhammad Asraf Mansor

Universiti Teknologi Malaysia

Mohd Ridzuan Ahmad (✉ mdridzuan@utm.my)

Universiti Teknologi Malaysia

Michal Petrů

Technical University of Liberec

Seyed Saeid Rahimian Koloor

Technical University of Liberec

Research Article

Keywords: Single cell analysis, impedance analysis, microfluidic, impedance flow cytometry

Posted Date: May 20th, 2022

DOI: <https://doi.org/10.21203/rs.3.rs-1660328/v1>

License:  This work is licensed under a Creative Commons Attribution 4.0 International License.

[Read Full License](#)

An impedance flow cytometry with integrated dual microneedle for electrical properties characterization of single cell

Muhammad Asraf Mansor¹, Mohd Ridzuan Ahmad^{1,*}, Michal Petru², and Seyed Saeid Rahimian Koloor²

¹*Division of Control and Mechatronics Engineering, School of Electrical Engineering, Faculty of Engineering, Universiti Teknologi Malaysia, 81310 Skudai, Johor, Malaysia*

²*Institute for Nanomaterials, Advanced Technologies and Innovation, Technical University of Liberec, Studentska 2, 461 17 Liberec, Czech Republic*

Abstract

Electrical characteristics of living cells have been proven to reveal important details about their internal structure, charge distribution, and composition changes in the cell membrane, as well as the extracellular context. An impedance flow cytometry is a common approach to determine the electrical properties of a cell, having the advantage of label-free and high throughput. However, the current techniques are complex and costly for the fabrication process. For that reason, we introduce an integrated dual microneedle-microchannel for single-cell detection and electrical properties extraction. The dual microneedles utilized a commercially-available Tungsten needle coated with parylene. When a single cell flows through the parallel facing electrode configuration of the dual microneedle, the electrical impedance at multiple frequencies is measured. The impedance measurement demonstrated the differential of normal red blood cells with three different sizes of microbeads at low and high frequencies, 100 kHz and 2 MHz, respectively. An electrical equivalent circuit model (ECM) was used to determine the unique membrane capacitance of individual cells. The proposed technique demonstrated that the specific membrane capacitance of an RBC is 9.42 mF/m², with the regression coefficients, ρ at 0.9895. As a result, this device may potentially be used in developing countries for low-cost single-cell screening and detection.

Keywords: Single cell analysis ; impedance analysis ; microfluidic ; impedance flow cytometry

Introduction

Label-free analysis in the microfluidic single-cell impedance technique is widely utilized for early cancer detection, disease development prediction, and therapeutic intervention suggestions. The label-

free analysis technique is a significant study due to reflects with its cell phenotype, such as biophysical electrical or mechanical properties. It is label-free means that the cells are not changed by chemical reagents or by extensive handling [1]. This label-free method protects cells from adverse effects associated with label production and is helpful in a wide range of applications. Microfluidic impedance spectroscopy is one commonly employed label-free method that is capable to measures the electrical characteristics of cells. Electrokinetic techniques based on alternating current (AC), particularly electrorotation and/or dielectrophoresis, have been utilized in the past [2–4]. The AC electrokinetic approach is a powerful tool capable of extracting the electrical properties of the cell, however they lack high throughput, even though the recent approaches have improved this [5–7].

To address these limitations, a single-cell impedance cytometry technique was introduced, and it is now commonly utilized to determine the impedance of an individual cell [8–11]. Microfluidic impedance flow cytometry (IFC) is a well-established label-free and high throughput analysis technique, which is commonly used to determine the electrical properties of a cell. This technique allows for the investigation of single cells and cell-to-cell heterogeneity which is can be useful for early diagnosis of cancer, predicting disease progression and suggesting therapeutic interventions. Impedance flow cytometry determines the electric field screening of single cells moving through fabricated electrodes inside the microchannel by current change in response to an applied AC voltage over a range of frequencies (10 kHz - 50 MHz)(see Figure S1 in Supplementary Information). The impedance of system and properties of cell, such as volume and dielectric properties, influence the measurement signal of impedance flow cytometry.

An impedance flow cytometry was first introduced 70 years ago for bacteria detection in aerosols [12]. The development of the IFC is gained since it provides a rapid, non-invasive and real-time technique for detecting single cell biologically. Single-cell analysis utilizing IFC demonstrates the feasibility to identify undifferentiated and differentiated stem cells [13], by examining the electrical impedance ratio between two particular frequencies (a term known as opacity). Other studies have discovered that the IFC with platinum black electrode probe is capable of sensing the status of cells by measuring the impedance of cells at frequencies over 1 MHz [14]. The nanoneedle electrode embedded in the microchannel is used to detect the crossing of cells on the sensor area, enabling it to be sensitive to the solution's dielectric characteristics [15]. However, the fabrication procedure will be more expensive due to the patterning of the electrode nanoneedle on the substrate. Another drawback is the device's time-consuming cleaning process. Other researchers have introduced a microfluidic with constriction channel, which is a simple and high throughput technique to determine the electrical characteristics of a single cell (e.g. specific membrane capacitance) [16–19]. However, the microfluidic device with a constriction channel approach is difficult to optimize for size-heterogeneous samples.

Parallel, face-to-face microelectrodes configuration technique is common and widely utilized in impedance flow cytometry (IFC). The polystyrene beads (PS), red blood cells (RBCs), and RBCs in glutaraldehyde were compared in the microchannel with diameters between 20 and 30 microns to extract the dielectric characteristics of individual cells [20]. An impedance of individual cells was measured at two simultaneously applied frequencies; the magnitude, phase, and opacity index were utilized to differentiate cells. A substantial difference was seen in the opacity of the RBCs with fixed cell membranes. It also showed that cells could be accurately detected at around 500 kHz. Other works demonstrated a blood cell differential count using a microfluidic impedance-based IFC [21]. The results provide reliable impedance detection of T-lymphocytes, monocytes, and neutrophils by utilizing two frequencies and supported by simultaneous fluorescence measurements. The recent development of parallel electrode configuration shows five pairs of facing electrode was utilized to extract the parameter of electrical properties of cells at eight simultaneous frequencies measurement [22]. The cytoplasm conductivity and specific membrane capacitance of RBCs and ghost (no hemoglobin in the cytoplasm) were determined at a high throughput of around 400 cells/s and 200 cells/s for frequency sweep and single-cell spectroscopy, respectively. In addition, a similar electrode configuration has been utilized to investigate the pancreatic ductal adenocarcinoma (PDAC) tumor [23]. They

introduced a new phase contrast metric that shows systematic changes in the cell interior electrophysiology, that has been linked to cell tumorigenicity. However, fabricating facing electrodes necessitates sophisticated fabrication equipment and causes alignment challenges. On the other hand, patterning metal electrode probes on a silicon or glass substrate is a time-consuming process that adds to the impedance sensor's manufacturing cost.

Numerous groups have proved that utilizing a printed circuit board (PCB) as the measuring electrode minimises the cost of microfabricating electrodes [24]. They developed contactless electrode sensing in capillary electrophoresis [25] and cell manipulation using dielectrophoresis [26]. The electrode was built on the PCB substrate (reusable component), and sandwich with the thin bare dielectric substrate (e.g. thin glass cover and thin PDMS film), which was attached to the PDMS (Polydimethylsiloxane) microchannel (disposable component). The applied AC voltage applied at the electrodes can infiltrate the thin dielectric substrate to sense the presence of the cell. This method is capable of differentiating the WBCs and CTCs from the mixture sample [27]. Nevertheless, because the electric field is covered by the dielectric substrate, the penetration to the electrolyte is less and reduce the measurement sensitivity.

This paper demonstrates an integrated dual microneedles-microfluidic device for the single microbeads and RBCs in suspension detection and the membrane capacitance of RBCs estimation. The proposed IFC device is aim on minimizing the manufacturing cost while maintaining the device's primary functionality (i.e., single-cell detection). This study achieves a significant cost decrease in fabrication by utilizing a Tungsten microneedle as measurement electrodes. The Tungsten microneedle is reusable and quite easy to clean. Two Tungsten microneedles were located between the top and bottom of the disposable microchannel to sense and measure the impedance of cells flowing through an applied electric field [28,29]. The concept of facing electrodes configuration has been used because this approach generates a more homogeneous electric field distribution (but not perfectly uniform) and is more sensitive due to the electric field being restricted into a smaller detecting volume [10,30]. Three-dimensional electrode configuration is better effective for high sensing accuracy and sensitivity compared to the two-dimensional configuration [31,32]. The capability of the technique to extract the electrical properties of single red blood cells (RBCs) and microbeads was demonstrated. The impedance data are evaluated using the curve fitting of an electrical equivalent circuit model (ECM) with Maxwell's mixture equation and shell model to extract the electrical parameter of a single cell.

Theory

Impedance sensing is a technique that involves applying a frequency-dependent excitation signal to a system and measuring the response [33,34].

$$Z(\omega) = \frac{V(\omega)}{I(\omega)} = Z_{real} + j Z_{img} \quad (1)$$

Where ω is the frequency and $j=\sqrt{-1}$. $V(\omega)$ and $I(\omega)$ are the applied voltage and the response current, respectively. The dielectric characteristics of target cells and the host medium are reflected in the response current [30]. Resistance (Z_{real}) and reactance (Z_{img}) are the real and imaginary components of the complex impedance, respectively. The magnitude ($|Z|$) and phase angle (θ) of the complex impedance are;

$$|Z| = \sqrt{(Z_{real})^2 + (Z_{img})^2} \quad (2)$$

$$\theta = \tan^{-1} \frac{Z_{img}}{Z_{real}} \quad (3)$$

For this impedance flow cytometry, measurement involved cells flow in a conductive medium at multiple frequencies to obtain impedance spectra. These spectra are highly dependent on the dielectric properties of the cell, which could be used to determine the electrical parameter of a cell. Through fitting simulated impedance spectra to observed ones, ECM in combination with Maxwell's mixture theory and shell-models are often applied to achieve this goal [22,35].

Single-Shell Cell Electric Model

The electric model of a single cell in a liquid suspension is a popular theory and model of impedance-based measurement methods. There are several reviews for this model [8,30,32,36,37]. The single-shelled spherical model, which consists of a thin insulating shell (cell membrane) and conducting sphere (cytoplasm) (see Figure S2), is extensively utilized to evaluate impedance data [38,39]. When an alternating current electric field is introduced to a suspended cell, the dielectric characteristics of the cell vary as a function of frequency, which is known as Maxwell-Wagner dispersion. Maxwell's mixture theory is utilized to investigate the dielectric behavior of cell suspensions. The "single-shell" model is a fundamental model of a cell in suspension, where the cell membrane and the cytoplasm are modelled as the thin dielectric shell and the conducting homogenous sphere, respectively [40]. The single-shell model showed a good agreement with experimental data for cells with negligible nucleus or organelles. The details of MMT with a single shell model provide in section S2 of ESI [10,21,41].

The dielectric properties of the cell may be obtained by calculating its complex impedance at various frequencies. The common frequency range of the electric signals utilized in impedance measurement is in range 1 Hz to 10 GHz [42]. The frequency range has been divided into three separate dispersions (or relaxations), which have been labelled as α , β , and γ dispersions [43] and represents dielectric relaxations caused by polarisation processes in a complex biological environment (see Figure S3). The α -dispersion, frequencies below several kHz, is interfered by electrode polarization effects. Meanwhile, the β -dispersion is associated with the insulating cell membrane because of the interfacial polarization. The β -dispersion are commonly studied and utilized in impedance-based cell measuring technique because of several sub-dispersions dominated by the electric double layer effect, cell size, cell membrane, and cell cytoplasm [8,44,45]. The γ -dispersion is more than 1 GHz and generate by the reorientation of water molecules.

Equivalent Circuit Model for a Single-Shelled Cell Model

The equivalent circuit modeling (ECM) is widely used to extract system characteristics based on impedance measurement of multi-frequency datasets [46–48]. The advantage of using electrical circuit components to model the physical phenomena that make up a certain measured impedance response lies in the immediate recognizability of the elements and their frequency response, and consequently, in the inherent potential for standardized analysis. The assumption in the ECM is the electrical characteristics of a single cell (i.e., specific membrane capacitance) can be expressed using an equivalent circuit [30,49,50], as illustrated in Fig. 1. In general, the cell membrane resistance is significantly greater compared to its capacitance and may be neglected; similarly, the cytoplasm capacitance can be neglected because it is extremely lower compared to its resistance. The impedance of the suspending medium ($Z_{solution}$) is represented by the parallel of medium capacitance (C_{med}) and medium resistance (R_{med}), which are in series with electric double layer capacitance (C_{dl}) (Fig. 1(a)). In addition, when a single particle or cell flown through the sensing region, the cell is

approximated to a resistor that depicts the cytoplasm resistance (R_i) in series with capacitors that characterize the membrane capacitance (C_{mem}), as seen in Fig. 1(b). The total impedance magnitude of presence cell can be calculated using the equation:

$$Z_{cell} = \sqrt{(R_i)^2 + \frac{1}{(2\pi f C_{mem})^2}} \quad (4)$$

The capacitance electrical double-layer occurs at the contact between the electrode's surface and a liquid electrolyte beside it [51]. C_{dl} often grows in proportion to the surface area of electrode. Referring to the ECM concept, high C_{dl} and R_{med} can cause reduction of the observed cell and particle signals. As a result, electrodes with low capacitance electrical double-layer and high solution medium conductivity are advantageous for high sensitivity cell sensing. All value of these parameters contributing to total impedance is dependent on frequency (ω). The total impedance between two microelectrodes in the single-shell model is given by;

$$Z_{mix} = \frac{2}{j\omega C_{dl}} + \frac{R_{med}(1+j\omega R_i C_{mem})}{j\omega R_{med} C_{mem} + (1+j\omega R_i C_{mem})(1+j\omega R_{med} C_{med})} \quad (5)$$

where R_{med} , R_i , C_{mem} , and C_{med} represent the resistance of the medium, the resistance of cytoplasm, the capacitance of cell membrane, and the capacitance of medium, respectively.

The capacitive behavior of the cell plasma membrane is responsible for the frequency-dependent current that flows through the cell. Due to the large capacitance and low conductance of the plasma membrane, when the cell is exposed to a low-frequency electric field (10 kHz – 500 kHz), the plasma membrane acts as an insulator, preventing current from penetrating the cell cytoplasm and passing primarily around the cell [10,52]. At such frequencies, the membrane cell becomes polarized, which is hindering the electrical current penetration, and information about the cell size is gained [1]. The electrical double layer dominates the system impedance at a low frequency <100 kHz [10,36]. The membrane capacitance is completely short-circuited at higher frequencies, allowing the penetration of electric field inside the cytoplasm of the cell and allowing the intracellular characteristics to be studied, for example, specific membrane capacitance (1-5 MHz) (Fig. 1(c)) and cytoplasm conductivity (>10 MHz) [23]. By fitting the measured impedance spectra to respective equivalent circuits, the values of all-electric elements (i.e., membrane capacitance (C_{mem}) and cytoplasm resistance (R_i)) in the equivalent circuits were obtained. Thus, the C_{mem} value can be utilized to determine the specific membrane capacitance (C_{smem}) of the cell. The specific membrane capacitance is the membrane capacitance per unit surface area, which is an electrical characteristic that varies with the cell's physiological condition. The C_{smem} of human RBCs have been studied extensively using impedance cytometry and are found to lie within a broad range C_{smem} is known to be in the range of 7–14 mF/m² [22,53]. These significant differences may be due to the manner in which the samples were prepared as well as the device system used to collect measurement. Based on the geometrical assumption, the specific membrane capacitance C_{smem} can be calculated according to:

$$C_{smem} = \frac{C_{mem}}{4\pi r^2} \quad (6)$$

where C_{mem} is the capacitance of the cell obtained from curve fitting and radius of a cell represented by r . The typical values for the dielectric parameters for the cell [53]:

$\epsilon_o = 8.854 \times 10^{-12} \text{ Fm}^{-1}$, $\epsilon_{med} = 80\epsilon_o$, $\sigma_{med} = 1.6 \text{ Sm}^{-1}$, $\epsilon_{mem} = 11\epsilon_o$, $d = 7 \text{ nm}$, $r = 3.5 \text{ }\mu\text{m}$, $D = 25 \text{ }\mu\text{m}$ and $g = 15 \text{ }\mu\text{m}$, where d , r , D and g are the membrane thickness of RBC, the radius of RBC, the diameter of the electrode, and the gap between the electrode, respectively.

To obtain the confidence level associated with the simulated ECM fitting result, a regression coefficient ρ measures the degree to which the measurement data match the estimated simulation parameters were used. $X_{est}(f_i)$ is estimated using the proposed ECM, and $X_{exp}(f_i)$ represents measurement data. The value of ρ around 1 indicates that the theoretical model and the measurement data in an agreement [54].

$$\rho = 1 - \left[\frac{\sum_i (X_{exp}(f_i) - X_{est}(f_i))^2}{\sum_i (X_{exp}(f_i))^2} \right] \quad (6)$$

Materials and methods

Cell Culture

In the present study, we used two sets of a sample which are polystyrene (PS) microbeads in Phosphate-buffered saline (PBS) and red blood cell (RBC) from whole blood. The (PS) microbeads with a diameter of 5 μm , 7 μm , and 10 μm (Polysciences, Inc.) were prepared in three samples of 1 x PBS solution. Before being inserted into the device, each sample was sonicated for at least two minutes to prevent the (PS) microbeads from aggregating. The number of cells was approximately 7×10^3 beads/mL for each sample.

The whole blood of a patient was collected from the blood bank at the university clinic of Universiti Teknologi Malaysia. The whole blood sample of 1 ml was centrifuged for 10 min at 2000 rpm to separate RBC from other components such as plasma and buffy coat. After centrifugation, the buffy coat and plasma were removed carefully. Then the RBC was washed three times in phosphate-buffered saline (PBS) with centrifuged for 2 minutes at 2000 rpm and removed the supernatant. Next, RBCs were resuspended in the PBS (conductivity = 1.6 Sm^{-1}) to obtain approximately 6×10^3 cells/mL per sample for minimizing the possibility of duplicates. Because the ratio of RBCs to WBCs in human blood is generally 1000:1, the existence of WBCs was assumed neglected in these samples. The RBC samples were utilized within 48 hours in this study and the diameter of RBC is in the range of 7-8 μm .

Device Fabrication

The microfluidic IFC device has been developed by using the standard lithography method. The masks were designed using a layout editing tool (LayoutEditor, 2020, Juspertor GmbH). Then laser lithography equipment (PG501, Heidelberg Instruments, Heidelberg, Germany) was utilized to create two masks (top mask and bottom mask) on the 2.5-inch chromium (Cr) masks. After mask fabrication, the top layer mould was first created based on the two-step lithography technique using SU-8 2025 negative photoresist (MicroChem). The first layer SU-8 was spin-coated on a silicon wafer to obtain a thickness of 25 μm with 4000 rpm spin speed for 30 seconds. Following pre-baking, the top layer Cr mask was used to expose the first layer of the microchannel by using a mask aligner (SussMicroTech MA-6, Germany) and followed by post-baking with development.

Next, using 1500 rpm spin speed for 30 seconds, the second layer of SU-8 with 60 μm thicknesses was developed on the first layer microchannel and followed by pre-baked. Next, the substrate of the photoresist layer was aligned with the bottom layer Cr mask and exposed to UV light. Then the substrate was post-baked with development to produce a top mould master. After that, the bottom mould master with 60 μm thickness was fabricated by following the fabrication step of the top mould master. PDMS was prepared by thoroughly mixing PDMS pre-polymers (SYLGARD184A, Dow Corning Silicones Malaysia) with curing agents

(SYLGARD 184B, Dow Corning Silicones Malaysia, Malaysia) in a ratio of 9:1 by weight and poured on both SU-8 mould master. A PDMS microchannel was obtained after curing at 65°C for 2 hours in an oven (Isotherm, Esco, Singapore). The top and bottom sides of PDMS were cleaned with isopropyl (IPA) and sonicated for 10 minutes. Both clean PDMS microchannels were pre-heat on a hot plate for 5 minutes at a temperature of 120°. After pre-heat, both PDMS microchannels were treated with oxygen plasma (Plasma EtchPE-25, Plasma Etch, Inc., Carson City, NV, USA) for 25 seconds with oxygen at 10 cc/min to improve adhesion strength [29].

Both of the PDMS microchannels were sandwiched and post-heat for 15 minutes at a temperature of 120° to obtain the IFC device. The alignment of top and bottom PDMS microchannels was completed in less than two minutes to prevent loss of oxygen plasma effectiveness. The microchannel chip was completed by manual cutting using a flat knife and ruler at the right and left sides to leave a hole (60 µm × 120 µm) for the microneedle. A commercially-available tungsten needle (SE-20TB, Signatone, Gilroy, CA, USA) coated with parylene was utilized as a measuring electrode (two microneedles in total). The tip of the tungsten needle was trim by using the *Focused Ion Beam* -Scanning Electron Microscope (*FIB*-SEM) (Zeiss Crossbeam 340, Oberkochen, Germany) to obtain a flat tip surface with 25 µm diameter (see Figure S4). The length, shank diameter, and tip diameter of the Tungsten needle are 31.7 mm, 250 µm, and 25 µm, respectively. The configuration of dual microneedles was a parallel-facing electrodes design.

Experiment Setup

The inverted microscope (IX71, Olympus Corporation, Tokyo, Japan) was utilized to observe the sensing region of the IFC device. For observation and monitoring the presence of single cells/particles at sensing area, a high-speed camera (PROMON 501, AOS Technologies AG, Baden Daettwil, Switzerland) with GUI software (AOS imaging studio v4, AOS Technologies AG) has been utilized. Two tungsten microneedles were inserted into the IFC device through the square holes at both sides of the chip using a micromanipulator (EB-700, Everbeing, Taiwan) [28]. The gap of the microneedles was fixed at 15 µm. The alignment for the needles gap was obtained by measurement using imaging software (IC Measurement, The Imaging Source Asia Co., Ltd., Taiwan). The experimental setup is schematically represented in Fig. 2. As an input, the impedance analyzer (IM3570 Hioki, Nagano, Japan) was linked with two tungsten microneedles and shown on the computer. The syringe pumps (LEGATO 111, KD Scientific, Holliston, MA, USA) was used to control the microbeads and RBC samples. Two flexible silicon tubes (Silicon tubing, Malaysia) connected to the syringes and waste bottle were inserted into the PDMS device at the inlets for the introduction of liquids and outlet of waste liquids. The alignment for the needles gap was obtain by measurement using imaging software (IC Measurement, The Imaging Source Asia Co., Ltd., Taiwan)

Impedance Measurement Methods

To determine an object's unknown impedance, a known voltage across the object was applied, and the current flowing through it was recorded. A constant voltage excitation is better suitable for this application since the response current increases as the magnitude of the impedance decreases. Another advantage of utilizing a voltage source is that just the response current may be monitored, as steady voltage excitation in the appropriate frequency range is very straightforward to create [55]. Even though excitation voltage measurement is necessary for more precise IFC measurements, the complexity of the voltage source is much less than that of a current source. Initially, the characterization measurement and calibration of the IFC device was performed using 1 mL of the deionized (DI) water and phosphate-buffered saline (PBS). The frequency

sweep in the range of 10 kHz-3 MHz was used to provide no major shifts over the device impedance [28]. A syringe pump was set at a constant flow rate (6 $\mu\text{L}/\text{min}$) to drive each sample into the IFC microchannel. The impedance of both samples was measured five times.

Meanwhile, for single microbeads detection measurement, three samples of microbeads with a diameter of 5 μm , 7 μm and 10 μm were prepared for the measurement. The 1 mL of each sample flowed inside the IFC microchannel with 6 $\mu\text{L}/\text{min}$ of flow rate. An applied voltage of 1 Volt (V) AC signal with 7 frequencies measurement (10kHz, 50kHz, 100kHz, 500kHz, 800kHz, 1MHz and 2 MHz) is generated by impedance analyzer which was used to obtain the impedance of single cells/particles at the sensing area. The IFC microchannel device was washed with PBS for 3 minutes between each microbeads sample measurement. The data were collected using the GUI (graphical user interface) software (v3.10, Hioki E.E. Corporation, Nagano, Japan) of impedance analyzer, and post-processed in OriginPro (OriginLab Corporation, Northampton, MA, USA) and MATLAB (R2019b, MathWorks Inc., Natick, MA, USA).

Furthermore, the RBCs suspended in PBS (conductivity = 1.6 S m^{-1}) were injected into the IFC and driven along the IFC microchannel under the impact of applied pressure by syringe pumps at the flow rate of 6 $\mu\text{L}/\text{min}$. Several measurement frequency points were selected and approximately 50 cells per frequency were obtained. The measurement frequency was changed incrementally from 10kHz, 50kHz, 100kHz, 500kHz, 800kHz, 1MHz and 2 MHz, and the applied constant voltage was set at 1 V. The selected frequencies from 100 kHz to 2 MHz were used in this study, to concentrate on the impedance variations caused by the membrane lipid and to minimize the effect of electrical double-layer capacitance [56]. With the same procedure for microbead detection, the impedance of single RBCs was measured and collected.

Statistical analyses and curve fitting were performed using OriginPro and Zview (Scribner Associates Inc.). The results are presented in the form of mean \pm standard deviation or scatter plots. To perform the measurement, the impedance analyzer was self-calibrated before performing the measurement utilizing short and open standard calibration. Furthermore, to calibrate the IFC device, the impedance of a single microbead at a low frequency (100 kHz) has been measured to obtain the calibration curve. All the experiments were conducted with three microfluidic devices at room temperature for verify the device's repeatability.

Results and Discussion

Detection of Polystyrene (PS) Microbeads

The IFC device was first examined by a 7 μm diameter microbead to validate the sensing capability. The microbeads concentrations were in the range of $\sim 7 \times 10^2$ beads/mL. A time trace of 7 μm diameter microbeads travelling inside the IFC device with 6 $\mu\text{L}/\text{min}$ of flow rate is shown in Fig. 3. The results show that the single peak ($\sim 43.7 \pm 0.02 \times 10^4 \Omega$) is the signature of a single microbead (7 μm diameter) passing through a sensing area (dual tungsten needle) for a sample 5 microbeads captured at 500 kHz in one testing. The impedance magnitude threshold for 7 μm diameter microbead set at $42.0 \times 10^4 \Omega$, the lower than that considered as debris. As was verified optically, all the measured peaks corresponded to the microbeads through the sensing area. Afterwards, the IFC device was washed with DI water followed by PBS at a maximum flow rate (0.3 ml/min) before proceeding to the next experiment [28]. The sensitivity of the IFC device characterization is discussed in Section S.5 of Supplementary Information (Table S1 and Table S2).

For the calibration of the IFC device, each sample of PS microbeads (5 μm , 7 μm and 10 μm) and RBCs were mixed and suspended with 1x PBS solution at several of cell/bead approximately 5×10^2 cell/mL each sample. The calibration curve is used to experimental data measurement of the particles of interest (e.g.

RBCs). Fig. 4 illustrates the mix of both types of particles inside the IFC device. The mixed PS beads and RBCs sample was inserted into the device and flowed through the detection area to determine the magnitude of the impedance ($|Z|$) value based on cell size (volume) at a low frequency of 100 kHz with 6 $\mu\text{l}/\text{min}$ of flow rate. A good correlation is found between PS microbeads (5 μm , 7 μm and 10 μm) and RBCs at low-frequency impedance data (size). The result is shown in Fig. 5, where the mean \pm standard deviation of the PS microbeads and RBCs for approximately 50 individual events, measured at low frequency (100 kHz) is plotted as the size of particle versus impedance magnitude ($|Z|$). A calibration curve was obtained by fitting a second-order polynomial to the bead results [21]. Investigation of the low-frequency impedance data illustrates a significant overlap between 7 μm diameter microbead and RBCs, since the size of both particles is nearly the same diameters. The calibration curve has been utilized as a reference for red blood cell detection measurement based on the impedance of cell size. PS microbeads are commonly employed as benchmarks during IFC studies and should be electrically isolated at both high and low frequencies. Thus, a calibration using microbeads can serve as a standard for comparison with cells.

The experiment was performed three times to produce a consistent measurement, and each time using a new sample and a clean device. The measured microbeads impedance changes are in agreement with the calibration curve. It is well known as the IFC principle that under low excitation frequency, the impedance magnitude was measured based on the size of the particles [21,57]. We demonstrated that the magnitude of the impedance change is influenced significantly by the particle size at a low stimulation frequency of 100 kHz. The capability of impedance flow cytometry has been shown further by mixing three different sizes of microbeads. Due to the limit of available equipment setup, the IFC device was tested at the frequency range between 10 kHz to 2 MHz.

The mixing sample has flowed through the IFC microchannel, and the magnitude of the impedance was recorded at 7 frequency measurement. Fig. 6 shows well-differentiated spectrums of impedance magnitude in measured microbeads with a diameter of 5, 7, and 10 μm between 100 kHz and 2 MHz. As demonstrated, various sizes of microbeads can be distinguished by different impedance spectra. The impedance of PBS is used as a reference. The mean \pm standard deviation of the impedance magnitude represented each data point for approximately 50 individual events (each size of microbeads). The total data set depicted in the figure is the average frequency-dependent impedance of the sample. One set of measurements takes around 6 minutes to complete each size of microbeads, which has approximately 50 individual events. As shown in the Fig. 6, seven data sets of frequency measurement complete spectrum take 45 minutes to record. The impedance change ($\Delta Z = Z_{\text{mix}} - Z_{\text{solution}}$) of presence microbeads with absence microbeads was found to be linearly decreased with decreasing of frequency. In addition, the microbeads with different sizes can be clearly distinguished by the impedance magnitude changes at any frequency measurement. The individual impedance magnitude of each size of microbeads and RBCs at low frequency (100 kHz) and high frequency (2 MHz) has been shown in Supplementary Information (Figure S6 and Figure S7).

Detection of Human Red Blood Cells (RBCs)

To evaluate the performance of the fabricated IFC device for practical application in human cell detection, human RBCs were utilized because they are a readily available source of particles with generally homogenous and strong-defined dielectric characteristics. A sinusoidal voltage (1 V) with five frequencies measurement was applied to dual microneedles. The RBCs in PBS solution were pumped through the IFC device at a flow rate of 6 $\mu\text{l}/\text{min}$ and blocked the electric field which caused the current in the circuit loop to

drop (see Figure S8). The measured impedance change of medium was as an RBC detected at the sensing area. Thus, the impedance of each RBC detected event was obtained at five frequencies (100 kHz, 500 kHz, 800 kHz, 1 MHz, and 2 MHz) across two decades, thereby creating multiple single-cell datapoints. The frequency was purposely selected to minimize the effect of the electrical double layer (EDL) on the electrode surface, which leads to an increase in sensitivity. Fig. 7 shows the impedance magnitude profile of a single RBC pass through the dual microneedle within 5s. The circle at the peak of the signal indicated the RBCs pass through the sensing area. Approximate 4-5 RBCs passing through the sensing area are measured. Since the size of RBCs is in the range (6-8 μm), in this study, we only focus on impedance value of 7 μm diameter RBCs. In these experiments, the size of single RBCs was monitored by observation and through impedance measurement based on reference microbead. The impedance of 7 μm microbeads is used as reference particles because the microbeads have a fixed size distribution and consistent impedance throughout all measurement ranges [35,58]. As representative data, Figure 8(a) illustrates the mean \pm standard deviation of the total outcome of our experiment for RBC detection in the range of frequency 10 kHz to 2 MHz. Approximately 50 individual of RBCs impedances were recorded at 7 discrete frequencies. The impedance magnitude shows no significant difference at low frequencies (100 kHz). Meanwhile, increasing the frequency above 100 kHz, reduces the magnitude of the RBCs impedance because the RBCs are capacitive.

Furthermore, to discriminate the single RBCs with debris (e.g. PDMS debris and cell clusters), a threshold based on impedance change (ΔZ) of the sensing area due to the presence of the cell has been set. Figure 8(b) shows cells count based on the impedance change at a frequency measurement 500 kHz. The trigger width (green) sets the threshold for an accepted single RBC cell. The impedance change (ΔZ) of a single RBC lay between 3850 Ω to 3940 Ω . From the 63 detected peaks, 50 cells were identified based on the size and cell properties information obtained at the frequency of 500 kHz. Meanwhile, the rest are considered debris or clumping cells (ΔZ smaller or bigger than threshold width). In addition, the threshold for a single RBC at frequencies 10 kHz, 50 kHz, 100 kHz, 800 kHz, 1 MHz, and 2 MHz are presented in Figure S9.

Detection and Discrimination of RBCs with 7 μm Diameter Microbeads

To investigate discrimination capability, the impedance measurement of RBCs and 7 μm diameter microbeads was performed by a combination (1:1 ratio) of human RBCs and 7 μm diameter microbeads at low and high frequency, 100 kHz and 2 MHz, respectively. The mixture of RBCs and 7 μm diameter microbeads was inserted into the IFC device at a flow rate of 6 $\mu\text{l}/\text{m}$ and approximately 40 cells/particle was determined. In low frequencies (10 kHz - 500 kHz), the existence of an intact lipid membrane makes biological cells electrically insulating [59]. The impedance signal measured within this frequency range is associated with the cell size [14]. At high frequencies (1-5 MHz), the capacitance of the cell membrane causes a reactance peak in the imaginary component of the signal, which occurs directly before the membrane capacitance is effectively short-circuited [14]. The ratio of impedance magnitude at high to low frequency ($|Z|_{high}/|Z|_{low}$) or the so-called $|Z|$ opacity [21,30] provides a parameter that is independent of cell size, reflecting changes in the cell membrane. The cell membrane functioned as an insulator and screened current flow at low frequencies, as illustrated in Fig. 9. These results indicate that the impedance measurement was highly dependent on the cell volume. Due to the comparable sizes of the RBCs and 7 μm diameter microbeads, the observed impedance was near overlapped.

The cell membranes were transparent to the electric current when frequencies passed through dielectric relaxation, since the membrane capacitance could be pierced and therefore, the cell interior information was shown by the impedance measurement. Human RBCs exhibit β -dispersion with a typical relaxation frequency of about 1 MHz [60]. The relative opacities found in this IFC device at 2 MHz are 0.285 for RBCs and 0.345 for 7 μm diameter microbeads. As a result, the RBCs and 7 μm diameter microbeads could be differentiated at 2 MHz because the RBCs had larger cytoplasm conductivity than the non-conducting bulk material of the

beads [61]. Then we demonstrated the opacity of three different diameters of microbeads (5, 7, and 10 μm) with RBCs (see Figure S10 in Supplementary Information). It shows the correlation scatter plot of impedance magnitude measured at high and low frequencies for these three types of beads shows distinct clusters corresponding to the increased volume of the beads, and the fitting line with constant slope denotes the homogeneous dielectric properties of these beads made of the same material. The results are comparable with other reported works [20].

Determination of Specific Membrane Capacitance

The impedance magnitude spectra of PBS and RBCs as a function of frequency are shown in Fig. 10. The standard deviation is indicated by the error bar ($n=50$). In addition, because the electrical double layer capacitance electrode dominated the overall impedance in the low-frequency region ($\omega < 100$ kHz), while the cytoplasm characteristics can be determined at high-frequency region ($\omega > 10$ MHz) [62], we limited the frequency region between 100 kHz to 2 MHz to aim at the impedance variations produced by the membrane lipid and reduce the effect of the double-layer capacitance. The electrical double-layer capacitance minimization would lead to an increase in the measurement sensitivity [63]. The absence of cell, the impedance of PBS have three components, which are the medium resistance (R_{med}), medium capacitance (C_{med}) and electric double layer capacitance of electrode (C_{dl}) (see Figure 1(a)). The value of measured impedance magnitude at PBS is constant in the low frequency domains (55.2 ± 0.75 k Ω at 100 kHz), which can be modelled as a pure resistor (R_{med}). The average value are in agreement with previously published works [64,65]. The effect of electrical double layer (C_{dl}) set at 5.8 μF .

Meanwhile, the frequency of transition at which impedance magnitude begins to drop is around 100 kHz. The impedance magnitude decrease (15.5 ± 0.85 k Ω at 2 MHz) at high frequency domain, indicating the presence of a capacitance (C_{med}). The ECM without cell, was utilized to fit the measured impedance spectrum to determine the electric component of R_{med} and C_{med} . The obtained value of R_{med} and C_{med} are 57.6 ± 0.5 k Ω and 4.2 ± 0.4 pF, respectively, with all fitting regression coefficients higher than 0.99. As an RBC presence at the sensing area, the impedance magnitude of the system increase which is contributed from the RBCs in addition to R_{med} , C_{med} and C_{dl} . The impedance of the presence RBC can be modelled as a cytoplasm resistance (R_i) in series with membrane capacitance (C_{mem})(see Figure 1(b)) [63,66] and the total impedance can be determined by using equation 5. In addition, the impedance magnitude Z_{cell} can be calculated using the equation 4. The local ionic environment at the electrode/solution interface is also affected by the presence of cells, which can change the C_{med} and R_{med} and raise electrode impedance [67]. The value of measured impedance magnitude at RBCs is also constant at low-frequency domains (60.2 ± 0.75 k Ω at 100 kHz), modelled as two resistors R_{med} and R_i in parallel. Meanwhile at high frequency domains, a decrease in impedance magnitude occurred (17.2 ± 0.55 k Ω at 2 MHz). When an RBC was in the detection area, the impedance of the mixture medium was measured and fitted to ECM with cell to determine the R_i and C_{mem} . We tested RBC cells ($n=50$) with 5 frequency points, and the R_i and C_{mem} were determined to be 89.4 ± 0.5 k Ω and $1.45 \pm 0.05 \times 10^{-12}$ F, respectively, with all fitting the regression coefficients, ρ at 0.9895. The consistency between the measured and fitted impedance spectra demonstrated the viability of the equivalent circuit for reflecting the impedance characteristics of the IFC device with and without cell. Table 1 shows the simulated values of all electric elements in the ECM (with and without cell), R_{med} , C_{med} , C_{dl} , R_i and C_{mem} .

Leveraging equation 6, C_{mem} of RBCs was further translated to the specific membrane capacitance (C_{smem}) based on the geometrical assumption. The determined specific membrane capacitance C_{smem} is 9.42 mF/m² and the calculated values of this RBC cell fall into ranges reported by another IFC technique, for example, 7-14.3 mF/m² [22,68–70]. The membrane capacitance C_{mem} is of particular importance since the

characteristics of membranes can only be investigated through more sophisticated approaches like electron microscopy and chemical analysis otherwise. From the results, it can be concluded that the simulation of the proposed ECM with fitting electrical parameters is in agreement with experimental impedance data obtained by the IFC device at 5 frequencies measurement point.

Conclusion

The microfluidic IFC device rises as an efficient, environmentally friendly, and reliable tool to study single-cell suspension. Because cell membranes restrict low-frequency currents while passing high-frequency currents, measurements from several frequency domains will offer information on the membrane's and cytoplasm's dielectric characteristics. We demonstrated that a microfluidic IFC device could well be utilized to determine the dielectric characteristics of single red blood cells. These experiments reveal that the single RBC cell and single microbeads are successfully measured by a dual microneedle connected to an impedance analyzer. Its impedance was measured at frequencies of between 10 kHz and 2 Mhz. The reusable Tungsten microneedles are used as measure electrodes attached into the disposable PDMS microchannel.

Geometrical assumption and electrical equivalent models were developed to quantify the specific membrane capacitance from the experimental impedance data. The specific membrane capacitance was found to be in range, as reported in previous work. In addition, despite the lower fabrication cost, this device demonstrated the core functionality of the proposed sensor, which is to differentiate the RBCs and microbeads. Overall, we believe that the device is well suited for early cancer cell detection and water quality applications in developing countries since it considerably decreases manufacturing costs (by 20%, relying on facility leasing and raw material consumption).

Declaration of Competing Interest

This article does not contain any studies with human or animal subjects

Declaration of Competing Interest

The authors declare that they have no known competing financial interests or personal relationships that could have appeared to influence the work reported in this paper.

Acknowledgment

This project is supported by the Ministry of Higher Education of Malaysia and Universiti Teknologi Malaysia (grant no. Q.J130000.2851.00L23 and Q.J130000.21A2.04E82), as well as the Ministry of Education, Youth, and Sports of the Czech Republic and the European Union (European Structural and Investment Funds Operational Program Research, Development, and Education) in the framework of the project “Modular platform for autonomous chassis of specialized electric vehicles for freight and equipment transportation”, Reg. No. CZ.02.1.01/0.0/0.0/16_025/0007293. The projects support the fabrication of the devices and electrical system, measurement of the data, demonstration of the results, preparation and evaluation of the research draft, and the financial support for the official process of the publication. We would like to express our gratitude to Universiti Teknologi Malaysia and Technical University of Liberec for financing this research and providing continued support.

Author contributions

M.A.M. and M.R.A. are involved in research conceptualization and methodology, and fabrication of the integrated dual microneedles-microfluidic system. M.A.M., M.R.A., M.P., and S.S.R.K. involved in the design validity and visualization of the microchannel, and microfabrication and assembly of the electrodes, as well as analysis and demonstration of the three-dimensional electrode configuration. M.A.M., M.R.A., involved in the measurement of the electrical properties. M.A.M., M.R.A., M.P., and S.S.R.K. are involved in validation, visualization, formal analysis of the research, and the project administration. M.A.M., M.R.A., M.P., S.S.R.K., involved in the writing/review and editing of the original draft preparation of the manuscript. Supervision, resources, and funding acquisition of the project was managed by M.R.A., M.P. and S.S.R.K. All authors have read and agreed to the submitted version of the manuscript.

Appendix A. Supplementary material

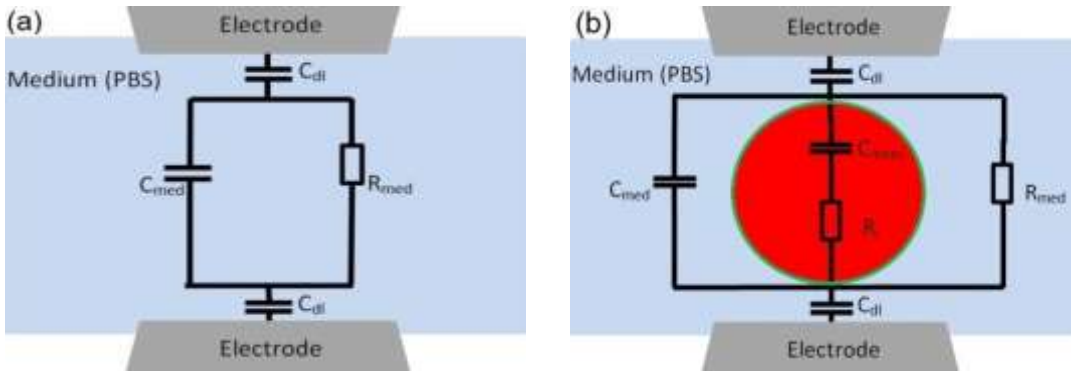
Table 1: Simulated value of the electrical element in the ECM for with and without RBC

	C_{dl} (μF)	R_{med} ($\text{k}\Omega$)	C_{med} (pF)	R_i ($\text{k}\Omega$)	C_{mem} (pF)	Z_{cell} (at 500 kHz) ^a ($\text{k}\Omega$)
PBS	5.8	57.6	4.2			
RBC	5.8	60.5	3.8	89.4	1.45	236.5

^a The impedance caused by the presence of a cell was calculated using the equation $Z_{cell} =$

$$\sqrt{(R_i)^2 + \frac{1}{(2\pi f C_{mem})^2}}$$

and a frequency measurement of 500 kHz.



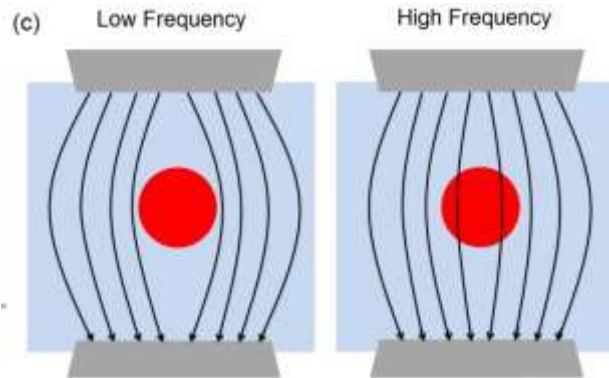


Fig. 1 (a) Schematic of ECM (without cell) used to fitting impedance spectrum with no cell passing ($Z_{solution}$), aiming to calculate the values of the medium capacitor (C_{med}) and medium resistor (R_{med}) (b) Schematic of ECM (with cell) to estimate the value of membrane capacitance (C_{mem}) and cytoplasm resistance (R_i) (“green” and “red” represent membrane and cytoplasm, respectively) by fitting with Z_{mix} measurement data. (c) The schematic of electric field penetration in cells with varying viability stages at low and high frequencies. In low frequency, the cell membrane acts as a substantial impediment to current penetration, allowing for the measuring of cell size. While in high frequency, the membrane polarization decreases and current may penetrate the cell membrane giving information of the membrane properties.

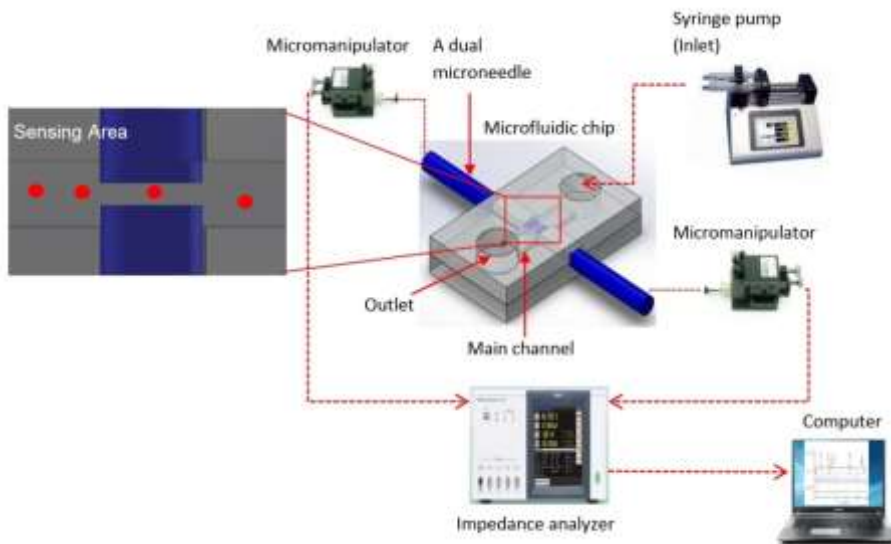


Fig. 2 The schematic diagram for the experiment. The micromanipulator used to hold and drive the Tungsten needles inside the microfluidic channel and the alignment of the needle gap was obtained using imaging software.

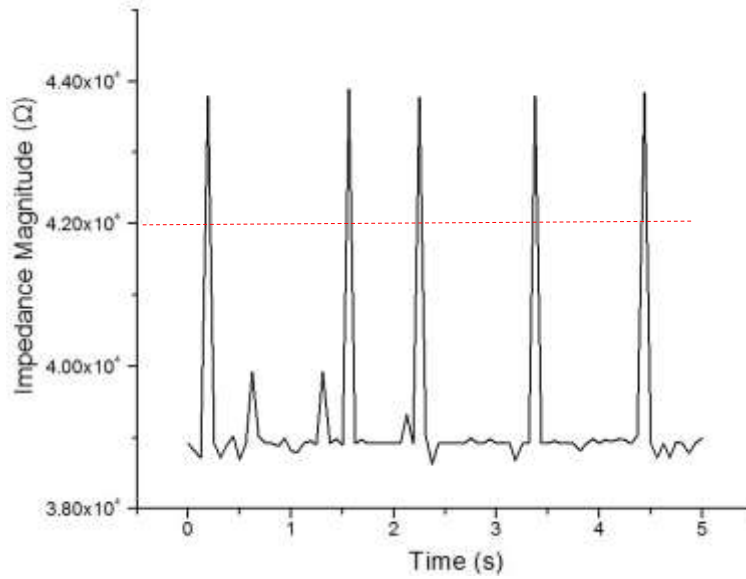


Fig. 3 The detection of microbeads of 7 μm size at detection area based on impedance change of the medium. Red dash line set as impedance magnitude threshold of 7 μm diameter microbeads and frequency measurement at 500 kHz.

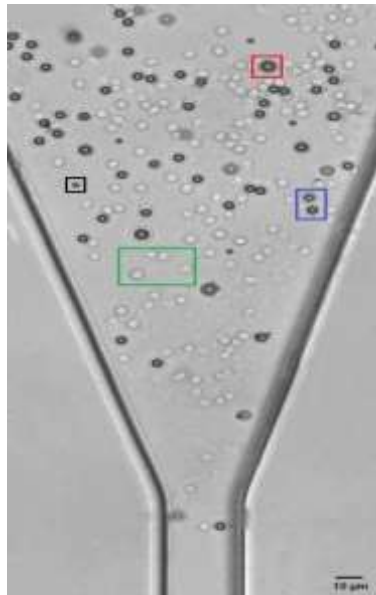


Fig. 4 The mixed PS beads and RBCs suspending inside microchannel of IFC device. (“green”, “black”, “blue” and “red” box represent RBCs, 5 μm microbead, 7 μm microbead and 10 μm microbead, respectively).

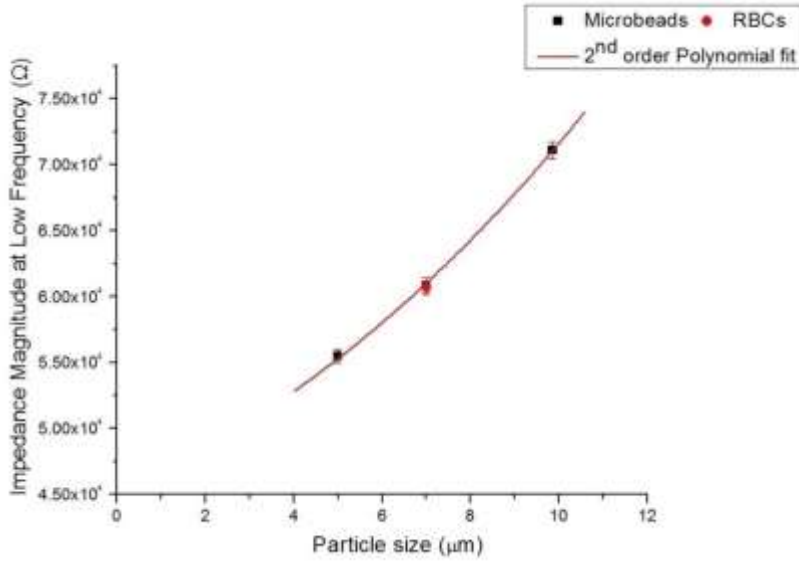


Fig. 5 Calibration data for the device at low-frequency measurement (100 kHz). Three different sizes of PS beads and RBCs were flowed inside the microchannel to measure the magnitude of the impedance and obtain the calibration curve. The calibration curve was utilized to determine the magnitude of impedance RBC.

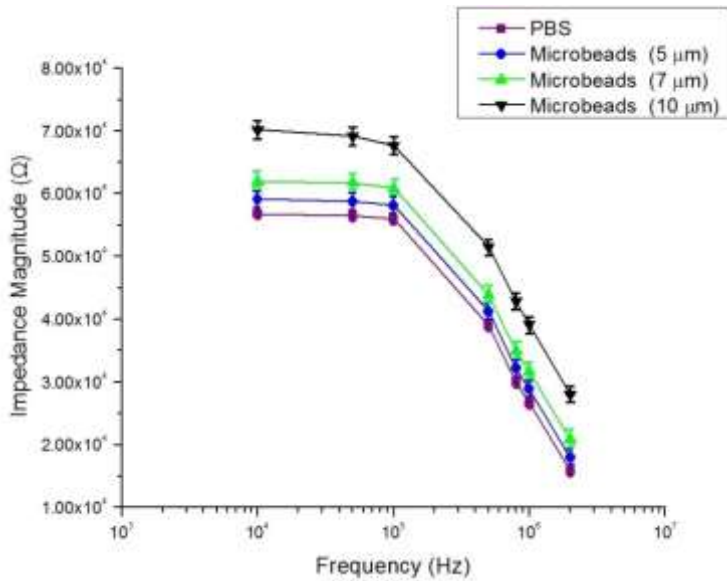


Fig. 6 Impedance Spectrum of 3 different sizes of microbeads (5 μm, 7 μm and 10 μm)

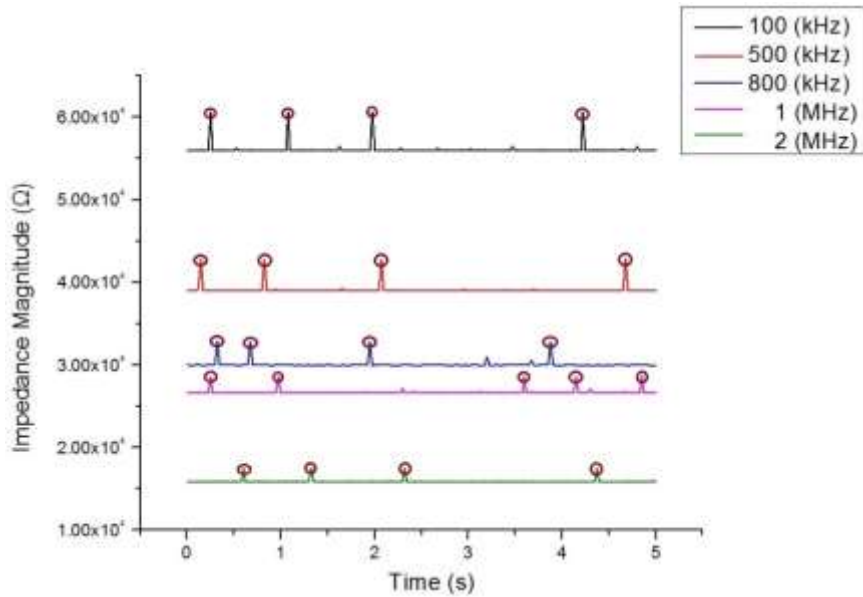


Fig. 7 Impedance magnitude profiles (at 5 frequencies) measured within 5s with 4-5 cells passing through the detection area. Impedance profiles of different frequencies are plotted in different colors.

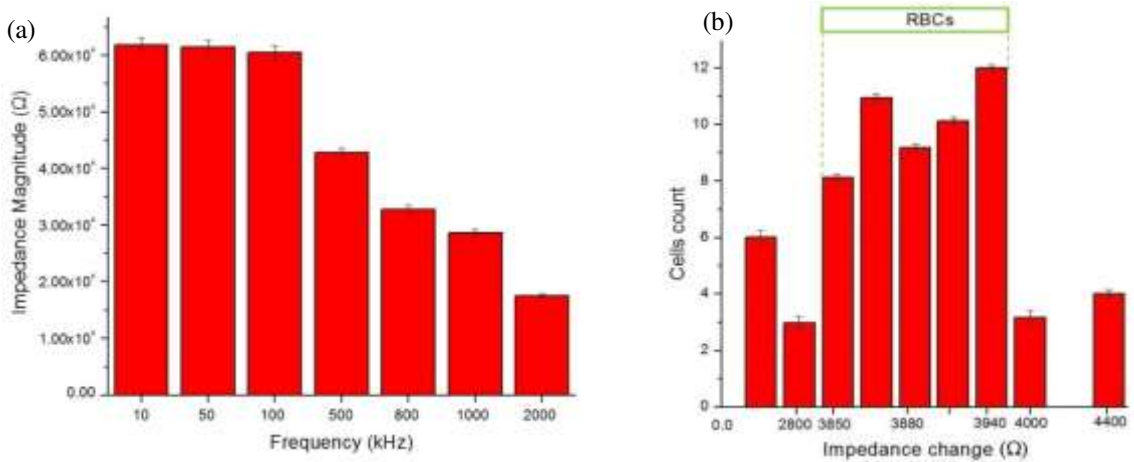


Fig. 8 (a) Total impedance spectrum of RBC at 7 frequencies measurement. With an increase in frequency, the measurable change in impedance decreases (b) Threshold for single-cell RBC based on impedance change (ΔZ) set in the range 3850 Ω to 3940 Ω based on data collected at 500 kHz.

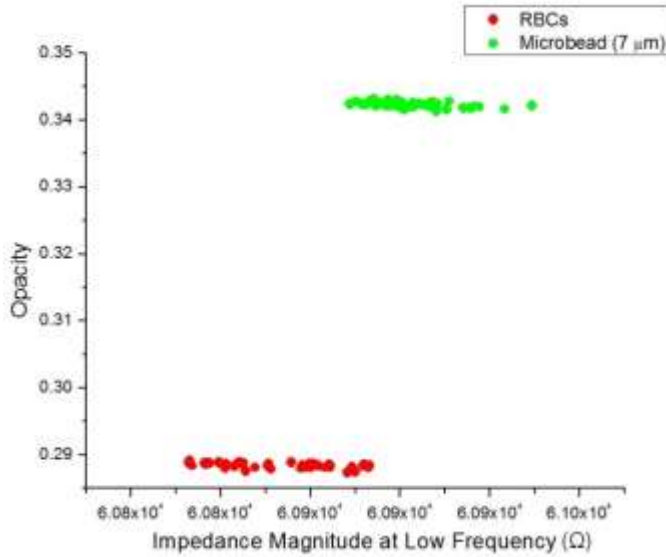


Fig. 9 Scatter plot of opacity against impedance magnitude at low frequency (100 kHz) for a mixture of RBCs and 7 μm diameter microbeads. Opacity is defined as the ratio of the high-frequency (100 kHz) to the low-frequency impedance, which indicates changes in the cell membrane and independent of cell size.

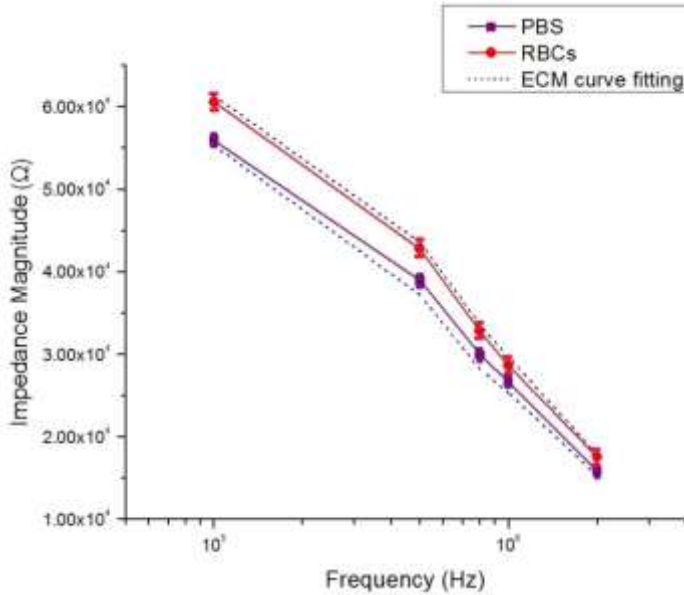


Fig. 10 Measurement impedance magnitude of PBS and RBCs at selected frequency point between 100 kHz – 2 MHz.

References

1. Ostermann M, Sauter A, Xue Y, Birkeland E, Schoelermann J, Holst B, et al. Label-free impedance flow cytometry for nanotoxicity screening. *Sci Rep*. 2020;10:1–14.
2. Yang J, Huang Y, Wang X, Wang XB, Becker FF, Gascoyne PR. Dielectric properties of human leukocyte subpopulations determined by electrorotation as a cell separation criterion. *Biophys J* [Internet]. 1999;76:3307–14. Available from: <http://www.pubmedcentral.nih.gov/articlerender.fcgi?artid=1300300&tool=pmcentrez&rendertype=abstract>
3. Han S-I, Joo Y-D, Han K-H. An electrorotation technique for measuring the dielectric properties of cells with simultaneous use of negative quadrupolar dielectrophoresis and electrorotation. *Analyst* [Internet]. 2013 [cited 2014 Sep 24];138:1529–37. Available from: <http://www.ncbi.nlm.nih.gov/pubmed/23353873>
4. Hölzel R. Non-invasive determination of bacterial single cell properties by electrorotation. *Biochim Biophys Acta* [Internet]. 1999;1450:53–60. Available from: <http://www.ncbi.nlm.nih.gov/pubmed/10231555>
5. M. D. Vahey and J. Voldman. An equilibrium method for continuous-flow cell sorting using dielectrophoresis. *Anal Chem*. 2008;80:3135–3143.
6. Xie X, Zhang Z, Ge X, Zhao X, Hao L, Cheng Z, et al. Particle Self-Aligning, Focusing, and Electric Impedance Microcytometer Device for Label-Free Single Cell Morphology Discrimination and Yeast Budding Analysis. *Anal Chem* [Internet]. 2019;91:13398–406. Available from: <https://pubs.acs.org/doi/10.1021/acs.analchem.9b01509>
7. Liu J, Qiang Y, Alvarez O, Du E. Electrical impedance microflow cytometry with oxygen control for detection of sickle cells. *Sensors Actuators, B Chem*. 2018;255:2392–8.
8. Sun T, Morgan H. Single-cell microfluidic impedance cytometry: a review. *Microfluid Nanofluidics* [Internet]. 2010 [cited 2014 Mar 19];8:423–43. Available from: <http://link.springer.com/10.1007/s10404-010-0580-9>
9. Mansor MA, Ahmad MR. Single Cell Electrical Characterization Techniques. *Int J Mol Sci* [Internet]. 2015;16:12686–712. Available from: <http://www.mdpi.com/1422-0067/16/6/12686/>
10. Honrado C, Bisegna P, Swami NS, Caselli F. Single-cell microfluidic impedance cytometry: From raw signals to cell phenotypes using data analytics. *Lab Chip*. 2021;21:22–54.
11. Cheung KC, Di Berardino M, Schade-Kampmann G, Hebeisen M, Pierzchalski A, Bocsi J, et al. Microfluidic impedance-based flow cytometry. *Cytometry A* [Internet]. 2010 [cited 2014 Sep 11];77:648–66. Available from: <http://www.ncbi.nlm.nih.gov/pubmed/20583276>
12. Gucker FT, O’Konski CT, Pickard HB, Pitts JN. A Photoelectronic Counter for Colloidal Particles. *J Am Chem Soc* [Internet]. 1947;69:2422–31. Available from: <https://pubs.acs.org/doi/abs/10.1021/ja01202a053>
13. Song H, Wang Y, Rosano JM, Prabhakarparandian B, Garson C, Pant K, et al. A microfluidic impedance flow cytometer for identification of differentiation state of stem cells. *Lab Chip* [Internet]. 2013;13:2300–10. Available from: <http://www.ncbi.nlm.nih.gov/pubmed/23636706>
14. Gawad S, Schild L, Renaud PH. Micromachined impedance spectroscopy flow cytometer for cell analysis and particle sizing. *Lab Chip*. 2001;1:76–82.
15. Esfandyarpour R, Javanmard M, Koochak Z, Harris JS, Davis RW. Nanoelectronic impedance detection of target cells. *Biotechnol Bioeng* [Internet]. 2014 [cited 2014 Aug 20];111:1161–9. Available from: <http://www.ncbi.nlm.nih.gov/pubmed/24338648>
16. Zhao Y, Liu Q, Sun H, Chen D, Li Z, Fan B, et al. Electrical property characterization of neural stem cells in differentiation. *PLoS One*. 2016;11:1–12.
17. Han Z, Chen L, Zhang S, Wang J, Duan X. Label-Free and Simultaneous Mechanical and Electrical Characterization of Single Plant Cells Using Microfluidic Impedance Flow Cytometry. *Anal Chem*. 2020;92:14568–75.
18. Wang K, Zhao Y, Chen D, Fan B, Lu Y, Chen L, et al. Specific membrane capacitance, cytoplasm conductivity and instantaneous Young’s modulus of single tumour cells. *Sci Data* [Internet]. 2017;4:170015.

Available from: <http://www.nature.com/articles/sdata201715>

19. Zhao Y, Chen D, Luo Y, Chen F, Zhao X, Jiang M, et al. Simultaneous Characterization of Instantaneous Young's Modulus and Specific Membrane Capacitance of Single Cells Using a Microfluidic System. *Sensors* [Internet]. 2015;15:2763–73. Available from: <http://www.mdpi.com/1424-8220/15/2/2763/>
20. Cheung K, Gawad S, Renaud P. Impedance spectroscopy flow cytometry: On-chip label-free cell differentiation. *Cytom Part A* [Internet]. 2005 [cited 2014 Nov 4];65:124–32. Available from: <http://www.ncbi.nlm.nih.gov/pubmed/15825181>
21. Holmes D, Pettigrew D, Recciusi CH, Gwyer JD, van Berkel C, Holloway J, et al. Leukocyte analysis and differentiation using high speed microfluidic single cell impedance cytometry. *Lab Chip* [Internet]. 2009 [cited 2014 Oct 17];9:2881–9. Available from: <http://www.ncbi.nlm.nih.gov/pubmed/19789739>
22. Spencer D, Morgan H. High-Speed Single-Cell Dielectric Spectroscopy. *ACS Sensors*. 2020;5:423–30.
23. McGrath JS, Honrado C, Moore JH, Adair SJ, Varhue WB, Salahi A, et al. Electrophysiology-based stratification of pancreatic tumorigenicity by label-free single-cell impedance cytometry. *Anal Chim Acta* [Internet]. Elsevier Ltd; 2020;1101:90–8. Available from: <https://doi.org/10.1016/j.aca.2019.12.033>
24. Emaminejad S, Javanmard M, Dutton RW, Davis RW. Microfluidic diagnostic tool for the developing world: contactless impedance flow cytometry. *Lab Chip*. 2012;12:4499.
25. Wang J, Chatrathi MP, Mulchandani A, Chen W. Capillary electrophoresis microchips for separation and detection of organophosphate nerve agents. *Anal Chem* [Internet]. 2001;73:1804–8. Available from: <http://www.ncbi.nlm.nih.gov/pubmed/11338594>
26. Park K, Suk H-J, Akin D, Bashir R. Dielectrophoresis-based cell manipulation using electrodes on a reusable printed circuit board. *Lab Chip*. 2009;9:2224–9.
27. Fu Y, Yuan Q, Guo J. Lab-on-PCB-based micro-cytometer for circulating tumor cells detection and enumeration. *Microfluid Nanofluidics*. Springer Berlin Heidelberg; 2017;21:1–4.
28. Mansor MA, Takeuchi M, Nakajima M, Hasegawa Y, Ahmad M. Electrical Impedance Spectroscopy for Detection of Cells in Suspensions Using Microfluidic Device with Integrated. *Appl Sci* [Internet]. 2017;7:170. Available from: <http://www.mdpi.com/2076-3417/7/2/170>
29. Mansor MA, Takeuchi M, Nakajima M, Hasegawa Y, Ahmad MR. A novel integrated dual microneedle-microfluidic impedance flow cytometry for cells detection in suspensions. *Int J Electr Comput Eng* [Internet]. 2017;7:1513. Available from: <http://www.iaescore.com/journals/index.php/IJECE/article/view/7517>
30. Morgan H, Sun T, Holmes D, Gawad S, Green NG. Single cell dielectric spectroscopy. *J Phys D Appl Phys*. 2007;40:61–70.
31. Petchakup C, Li H, Hou HW. Advances in single cell impedance cytometry for biomedical applications. *Micromachines*. 2017;8.
32. Zhu S, Zhang X, Zhou Z, Han Y, Xiang N, Ni Z. Microfluidic impedance cytometry for single-cell sensing: Review on electrode configurations. *Talanta* [Internet]. 2021;233:122571. Available from: <https://linkinghub.elsevier.com/retrieve/pii/S0039914021004926>
33. Sun T, Green NG, Gawad S, Morgan H. Analytical electric field and sensitivity analysis for two microfluidic impedance cytometer designs. *IET Nanobiotechnol* [Internet]. 2007 [cited 2014 Jul 15];1:69–79. Available from: <http://www.ncbi.nlm.nih.gov/pubmed/17764376>
34. Holmes D, Morgan H. Single cell impedance cytometry for identification and counting of CD4 T-cells in human blood using impedance labels. *Anal Chem* [Internet]. 2010;82:1455–61. Available from: <http://www.ncbi.nlm.nih.gov/pubmed/20104894>
35. Honrado C, Ciuffreda L, Spencer D, Ranford-Cartwright L, Morgan H. Dielectric characterization of Plasmodium falciparum-infected red blood cells using microfluidic impedance cytometry. *J R Soc Interface*. 2018;15.
36. Xu Y, Xie X, Duan Y, Wang L, Cheng Z, Cheng J. A review of impedance measurements of whole cells. *Biosens Bioelectron*. Elsevier B.V.; 2016;77:824–36.
37. Balakrishnan SG, Ahmad MR, Kooloor SSR, Petru M. Separation of ctDNA by superparamagnetic bead

- particles in microfluidic platform for early cancer detection. *J Adv Res* [Internet]. 2021;33:109–16. Available from: <https://linkinghub.elsevier.com/retrieve/pii/S2090123221000369>
38. Asami K. Characterization of heterogeneous systems by dielectric spectroscopy. *Prog Polym Sci* [Internet]. 2002;27:1617–59. Available from: <https://linkinghub.elsevier.com/retrieve/pii/S0079670002000151>
39. Asami K. Dielectric dispersion in biological cells of complex geometry simulated by the three-dimensional finite difference method. *J Phys D Appl Phys* [Internet]. 2006;39:492–9. Available from: <https://iopscience.iop.org/article/10.1088/0022-3727/39/3/012>
40. Fricke H. A Mathematical Treatment of the Electric Conductivity and Capacity of Disperse Systems ii. The Capacity of a Suspension of Conducting Spheroids Surrounded by a Non-Conducting Membrane for a Current of Low Frequency. *Phys Rev* [Internet]. 1925;26:678–81. Available from: <https://link.aps.org/doi/10.1103/PhysRev.26.678>
41. Nasir N, Al Ahmad M. Cells Electrical Characterization: Dielectric Properties, Mixture, and Modeling Theories. *J Eng (United Kingdom)*. 2020;2020.
42. Asami K. Characterization of biological cells by dielectric spectroscopy. 2002;305:268–77.
43. P.Schwan H. Electrical Properties of Tissue and Cell Suspensions. *Adv Biol Med Phys*. 1957;5:147–209.
44. Sun T, Holmes D, Gawad S, Green NG, Morgan H. High speed multi-frequency impedance analysis of single particles in a microfluidic cytometer using maximum length sequences. *Lab Chip* [Internet]. 2007 [cited 2014 May 26];7:1034–40. Available from: <http://www.ncbi.nlm.nih.gov/pubmed/17653346>
45. SUN T, GREEN NG, MORGAN H. ANALYTICAL AND NUMERICAL MODELING METHODS FOR IMPEDANCE ANALYSIS OF SINGLE CELLS ON-CHIP. *Nano* [Internet]. 2008;03:55–63. Available from: <https://www.worldscientific.com/doi/abs/10.1142/S1793292008000800>
46. Lin Z, Lin SY, Xie P, Lin CY, Rather GM, Bertino JR, et al. Rapid Assessment of Surface Markers on Cancer Cells Using Immuno-Magnetic Separation and Multi-frequency Impedance Cytometry for Targeted Therapy. *Sci Rep*. 2020;10:1–10.
47. Fan W, Chen X, Ge Y, Jin Y, Jin Q, Zhao J. Single-cell impedance analysis of osteogenic differentiation by droplet-based microfluidics. *Biosens Bioelectron* [Internet]. 2019;145:111730. Available from: <https://linkinghub.elsevier.com/retrieve/pii/S0956566319308097>
48. Li H, Multari C, Palego C, Ma X, Du X, Ning Y, et al. Differentiation of live and heat-killed *E. coli* by microwave impedance spectroscopy. *Sensors Actuators, B Chem* [Internet]. Elsevier B.V.; 2018;255:1614–22. Available from: <https://doi.org/10.1016/j.snb.2017.08.179>
49. Foster KR, Schwan HP. Dielectric properties of tissues and biological materials: a critical review. *Crit Rev Biomed Eng* [Internet]. 1989;17:25–104. Available from: <http://www.ncbi.nlm.nih.gov/pubmed/2651001>
50. Zhao Y, Zhao XT, Chen DY, Luo YN, Jiang M, Wei C, et al. Tumor cell characterization and classification based on cellular specific membrane capacitance and cytoplasm conductivity. *Biosens Bioelectron* [Internet]. Elsevier; 2014 [cited 2014 May 27];57:245–53. Available from: <http://dx.doi.org/10.1016/j.bios.2014.02.026>
51. Iqbal SMA, Butt NZ. Design and analysis of microfluidic cell counter using spice simulation. *SN Appl Sci* [Internet]. Springer International Publishing; 2019;1:1–10. Available from: <https://doi.org/10.1007/s42452-019-1327-1>
52. S. Grimnes and O. G. Martinsen. *Bioimpedance and bioelectricity basics*. Academic press; 2000.
53. Mahesh K, Varma M, Sen P. Double-peak signal features in microfluidic impedance flow cytometry enable sensitive measurement of cell membrane capacitance. *Lab Chip*. 2020;20:4296–309.
54. Chan K., Morgan H, Morgan E, Cameron I, Thomas M. Measurements of the dielectric properties of peripheral blood mononuclear cells and trophoblast cells using AC electrokinetic techniques. *Biochim Biophys Acta - Mol Basis Dis* [Internet]. 2000;1500:313–22. Available from: <https://linkinghub.elsevier.com/retrieve/pii/S0925443999001155>
55. Ojarand J, Min M, Koel A. Multichannel Electrical Impedance Spectroscopy Analyzer with Microfluidic

Sensors. Sensors (Basel). 2019;19.

56. Chen L, Han Z, Fan X, Zhang S, Wang J, Duan X. An impedance-coupled microfluidic device for single-cell analysis of primary cell wall regeneration. *Biosens Bioelectron* [Internet]. Elsevier B.V.; 2020;165:112374. Available from: <https://doi.org/10.1016/j.bios.2020.112374>

57. Zheng S, Liu M, Tai YC. Micro coulter counters with platinum black electroplated electrodes for human blood cell sensing. *Biomed Microdevices*. 2008;10:221–31.

58. Spencer D, Hollis V, Morgan H. Microfluidic impedance cytometry of tumour cells in blood. *Biomicrofluidics* [Internet]. 2014;8:064124. Available from: <http://aip.scitation.org/doi/10.1063/1.4904405>

59. Tan Q, Ferrier GA, Chen BK, Wang C, Sun Y. Quantification of the specific membrane capacitance of single cells using a microfluidic device and impedance spectroscopy measurement. *Biomicrofluidics* [Internet]. 2012;6:34112. Available from: <http://www.ncbi.nlm.nih.gov/pubmed/23940502>

60. Bone S, Ginzburg BZ, Morgan H, Wilson G, Zaba B. Time-domain dielectric spectroscopy applied to cell suspensions. *Phys Med Biol* [Internet]. 1993;38:511–20. Available from: <https://iopscience.iop.org/article/10.1088/0031-9155/38/4/003>

61. Han C, Liang Z, Yu D, Xing X. A Single-Cell Impedance Micro-Cytometer Featuring 3D Electro-Fluidic Structures Monolithically Integrated Within Silver Pdms. 2019 20th Int Conf Solid-State Sensors, Actuators Microsystems Eurosensors XXXIII, TRANSDUCERS 2019 EUROSENSORS XXXIII. IEEE; 2019;9–12.

62. McGrath JS, Honrado C, Spencer D, Horton B, Bridle HL, Morgan H. Analysis of Parasitic Protozoa at the Single-cell Level using Microfluidic Impedance Cytometry. *Sci Rep* [Internet]. IEEE; 2017;7:2601. Available from: <http://ieeexplore.ieee.org/document/7863645/>

63. Feng Y, Huang L, Zhao P, Liang F, Wang W. A Microfluidic Device Integrating Impedance Flow Cytometry and Electric Impedance Spectroscopy for High-Efficiency Single-Cell Electrical Property Measurement. *Anal Chem*. 2019;91:15204–12.

64. Cho S, Thielecke H. Micro hole-based cell chip with impedance spectroscopy. *Biosens Bioelectron* [Internet]. 2007 [cited 2014 Oct 28];22:1764–8. Available from: <http://www.ncbi.nlm.nih.gov/pubmed/17008086>

65. Chen J, Zheng Y, Tan Q, Zhang YL, Li J, Geddie WR, et al. A microfluidic device for simultaneous electrical and mechanical measurements on single cells. *Biomicrofluidics* [Internet]. 2011 [cited 2014 Jun 30];5:14113. Available from: <http://www.pubmedcentral.nih.gov/articlerender.fcgi?artid=3082353&tool=pmcentrez&rendertype=abstract>

66. Jang L-S, Wang M-H. Microfluidic device for cell capture and impedance measurement. *Biomed Microdevices* [Internet]. 2007 [cited 2014 Mar 19];9:737–43. Available from: <http://www.ncbi.nlm.nih.gov/pubmed/17508285>

67. Mamouni J, Yang L. Interdigitated microelectrode-based microchip for electrical impedance spectroscopic study of oral cancer cells. *Biomed Microdevices* [Internet]. 2011 [cited 2014 Apr 29];13:1075–88. Available from: <http://www.ncbi.nlm.nih.gov/pubmed/21833766>

68. Asami K, Takahashi Y, Takashima S. Dielectric properties of mouse lymphocytes and erythrocytes. *Biochim Biophys Acta - Mol Cell Res* [Internet]. 1989;1010:49–55. Available from: <https://linkinghub.elsevier.com/retrieve/pii/0167488989901833>

69. Lisin R, Zion Ginzburg B, Schlesinger M, Feldman Y. Time domain dielectric spectroscopy study of human cells. I. Erythrocytes and ghosts. *Biochim Biophys Acta - Biomembr* [Internet]. 1996;1280:34–40. Available from: <https://linkinghub.elsevier.com/retrieve/pii/0005273695002669>

70. Gimsa J, Schnelle T, Zechel G, Glaser R. Dielectric spectroscopy of human erythrocytes: investigations under the influence of nystatin. *Biophys J* [Internet]. 1994;66:1244–53. Available from: <https://linkinghub.elsevier.com/retrieve/pii/S0006349594809087>

Supplementary Files

This is a list of supplementary files associated with this preprint. Click to download.

- [supplementary.docx](#)